ICPMG 2026

Proceedings of the 11th ICPMG 2026
11th International Conference on Physical Modelling in Geotechnics
8-12 June 2026, Zurich, Switzerland

Deep Excavation Behavior with Surface Load Components: Centrifuge and Numerical Analyses

Q. Abbas
Interdisciplinary Research Center for Construction and Building Materials, King Fahd University of Petroleum and Minerals, Dhahran 31261, Saudi Arabia, qaisar.abbas@kfupm.edu.sa

M. Aziz
Civil and Environmental Engineering Department, King Fahd University of Petroleum and Minerals, Dhahran 31261, Saudi Arabia, mubashir.aziz@kfupm.edu.sa

J. Yoon, M. Kim, M. Kim, J. Lee
Civil and Environmental Engineering Department, Yonsei University, Seoul, South Korea, yjh97@yonsei.ac.kr, zzzrlarlfkd@yonsei.ac.kr, mmmm9775@yonsei.ac.kr, junlee@yonsei.ac.kr

ABSTRACT: In this study, the effect of surface loading on wall and ground responses in deep excavation was examined. Centrifuge tests and finite-element analyses were conducted to assess the influence of loading position (e_s), area (A_{BL}) defined by width (B_s) and length (L_s), and load magnitude (Q). Results indicated that smaller e_s, larger A_{BL}, and higher Q resulted in larger wall deflection, ground settlement, and lateral earth pressure. These effects reduced near the greenfield condition at e_s/H_{ex}, B_s/H_{ex}, and L_s/H_{ex} of 1.2, 2.0, and 2.0, respectively. The impact of increasing B_s/H_{ex} was more pronounced than L_s/H_{ex}, showing directional sensitivity. A modified influence factor (η), based on stiffness influence factor (I_F), was proposed to quantify the effects of surface loading. Case studies verified the methods accuracy in predicting excavation responses under nearby surface loads.

1 INTRODUCTION

The demand for deep excavations in densely built urban areas has increased due to the construction of high-rise basements, cut-and-cover tunnels, underground parking, rail transit systems, and subsurface utilities (Ou et al. 2020; Giraldo and Bryson 2021; Abbas et al. 2025). These excavations are often carried out close to existing structures. As a result, excavation-induced wall deformation and ground settlement pose significant risks, leading to serviceability problems, structural damage, and economic and safety concerns (Li et al. 2018; Wang et al. 2024).

In urban environments, surface loads from adjacent buildings and construction activities can significantly amplify excavation-induced responses and modify wall and ground movement patterns compared with greenfield conditions (Son and Cording 2008; Ou et al. 2020). Typical excavation-induced movements and related components are described in Figure 1 (Hsieh and Ou 1998). Although previous studies have mainly focused on building response and damage assessment, the direct influence of surface loading configuration on excavation-induced wall and ground movements has not been fully quantified (Goh and Mair 2014; Maddah et al. 2021; Abbas et al. 2025).

This study investigates the effects of surface loading on wall deflection and ground settlement in deep excavations, considering variations in loading position (e_s), area (A_{BL}) defined by width (B_s) and length (L_s), and load magnitude (Q). Centrifuge tests combined with staged three-dimensional finite element analyses are used to quantify the relative influence of these loading components on excavation performance.

2 CENTRIFUGE EXPERIMENTS

2.1 Experiment description

A centrifuge testing program was established to investigate the effects of surface loading on δ_w and s_v associated with deep excavations. The tests were performed using a centrifuge with a aram length of 1.5 m and a rigid container (0.5 m × 0.2 m × 0.4 m). All experiments were carried out at an acceleration level of 50g. The dimensions of the centrifuge container were selected to minimize boundary effects relative to the excavation depth and loading width.

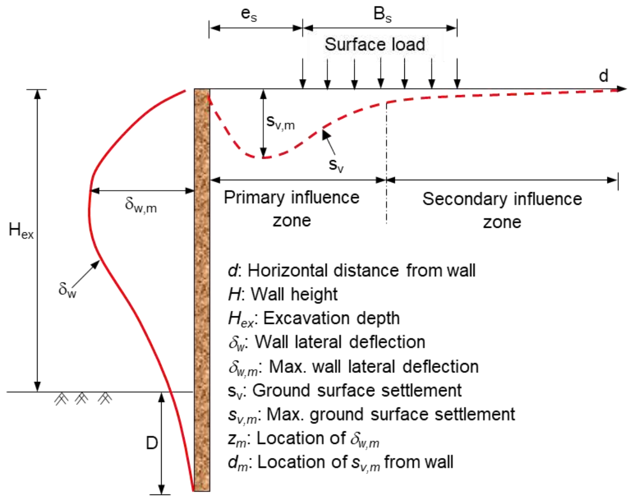

Figure 1. Typical excavation-induced movements and related components.

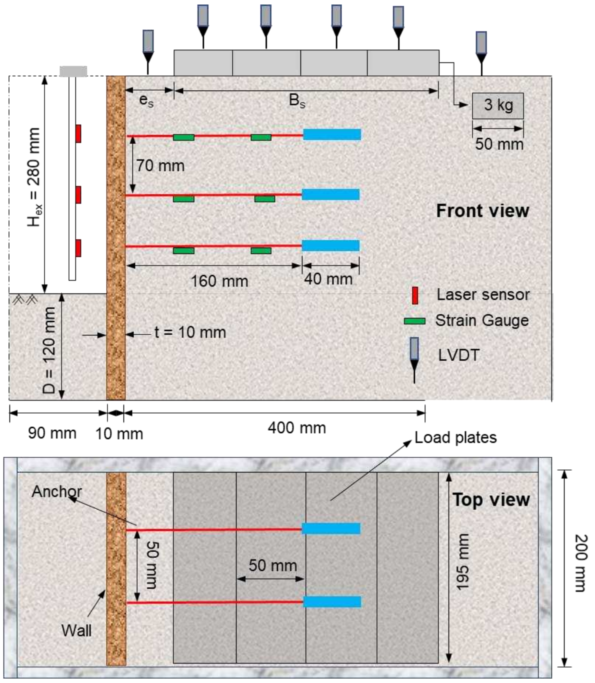

Figure 2. Configurations of centrifuge test setup.

The primary variables considered were the e_s and B_s, representing the load location and size, respectively. Five tests were conducted, including a greenfield case without surface loading, three tests with B_s = 10 m and varying e_s = 2.5, 4.0, and 5.5 m, and one test with an increased B_s = 15 m at e_s = 4.0 m.

The model wall was made of aluminum plate with a thickness and height of 10 mm and 400 mm (0.5 and 20 m in prototype), respectively. The wall was hinged at the base to allow rotation while preventing overturning. The excavation depth and embedment depth were 280 mm and 120 mm (14 and 6 m in prototype). Two rows of horizontal steel anchors were installed to support the wall and surface load was applied using steel plates. Wall deflection, surface settlement and anchor forces were measured using laser sensors, LVDTs and strain gauges, respectively. The soil specimen consisted of clean silica sand with the minimum and maximum dry densities ($\gamma_{d,min}$ and $\gamma_{d,max}$) of 16.46 and 18.82 kN/m^3, mean particle size (D_{50}) of 0.21 mm, uniformity coefficient (C_u) of 1.96, specific gravity (G_s) of 2.65 and internal friction angle (ϕ) of 36.4°. The sample prepared by air pluviation method with relative density (D_R) of 80%. The tests configurations and instrumentation adopted are shown in Figure 2.

2.2 Measured wall deflection and settlement

The centrifuge test results were obtained at the target acceleration level of 50g, with consistent initial conditions maintained to ensure reliable comparison of the results. The results indicate that surface loading significantly influences wall deflection (δ_w) and surface settlement (s_v) compared with the greenfield condition. Normalized wall deflection profiles (δ_w/H_{ex}) given in Figure 3, increased with decreasing e_s/H_{ex} and increasing B_s/H_{ex}. For e_s/H_{ex} values of 0.18, 0.28, and 0.39, the maximum wall deflection ($\delta_{w,m}/H_{ex}$) increased by approximately 56%, 42%, and 26%, respectively, compared to the greenfield case. For B_s/H_{ex} values of 0.71 and 1.07, $\delta_{w,m}/H_{ex}$ increased by about 42% and 46%, respectively. These results indicate that e_s/H_{ex} has a larger influence on δ_w than B_s/H_{ex}.

Surface settlement profiles (s_v/H_{ex}) exhibited a typical trough-shaped distribution behind the wall, with clear primary and secondary influence zones, as given in Figure 4. The maximum settlement ($s_{v,m}/H_{ex}$) increased by approximately 49%, 41%, and 37% for e_s/H_{ex} values of 0.18, 0.28, and 0.39, respectively, and by 41% and 47% for B_s/H_{ex} values of 0.71 and 1.07. Compared with the greenfield condition, surface loading significantly increased s_v, particularly within the secondary influence zone, indicating the combined

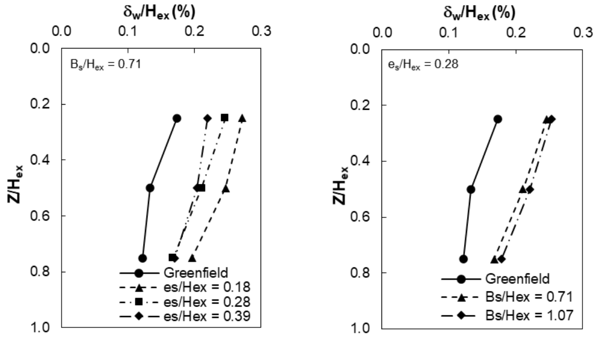

Figure 3. Measured wall deflection from centrifuge test.

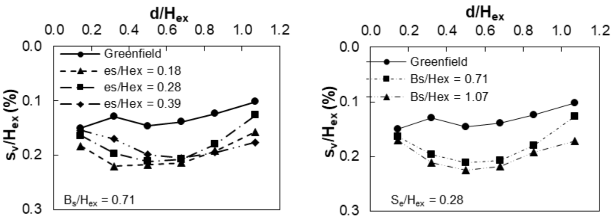

Figure 4. Measured settlement from centrifuge test.

effects of load proximity and loading area on excavation-induced ground movements. Centrifuge results show that both e_s/H_{ex} and B_s/H_{ex} significantly affect excavation response, with the influence of e_s/H_{ex} being more pronounced. However, due to the limited range of test conditions, further analyses are required to establish a comprehensive and generalizable quantification of surface loading effects.

3 NUMERICAL ANALYSIS

3.1 Analysis description

Three-dimensional finite element (FE) analyses were performed to further evaluate the effects of surface loading on wall and ground behavior under realistic field conditions and a wider range of loading configurations. The analyses were performed using PLAXIS 3D (V22) to simulate staged excavation while considering the key components of excavation behavior, including wall behavior, bracing systems, and construction sequence. A braced excavation system consisting of struts and walers was adopted, reflecting common urban conditions where ground anchors are often restricted. Surface loading component was e_s, loading area (A_{BL}) given by B_s and L_s, and load magnitude (Q), as described in Figure 5 and summarized in Table 1. The applied load was normalized by a reference value Q_{ref} = 30 kPa, representing typical 3-story building loads.

The FE domain measured 245 m × 230 m in plan with a depth of 60 m to minimize boundary effects. Soil was modelled using 10-noded tetrahedral elements with mesh refinement near the excavation. A 0.6 m thick diaphragm wall with an elastic modulus of 24.8 GPa was modelled using plate elements, while struts, walers, and center posts were simulated using beam elements with E = 210 GPa. The excavation depth (H_{ex}) and wall embedment depth (D) were 20 m and 10 m, respectively, with a rectangular excavation plan of 45 m × 30 m.

Table 1. FE analysis cases.

e_s/H_{ex}	B_s/H_{ex}	L_s/H_{ex}	Q/Q_{ref}
0.15, 0.30, 0.45, 0.60, 1.20	0.25, 0.5, 1.0, 1.5, 2.0	0.25, 0.5, 1.0, 1.5, 2.0	0.5, 1.0, 1.5, 2.0

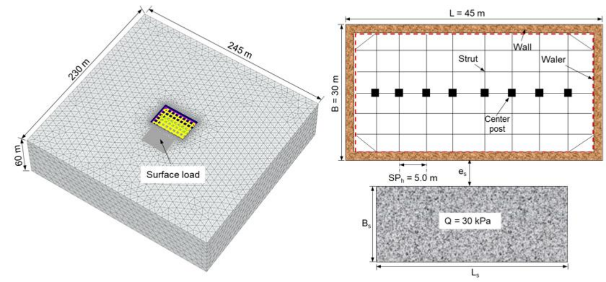

Figure 5. Description of FE model and parameters

Dense sandy soil was modeled as a drained material using the hardening soil model with small-strain stiffness (HSS), input properties are summarized in Table 2 (Brinkgreve et al. 2010; Zhang et al. 2019). Excavation was simulated in 14 stages with successive installation of struts and dewatering during excavation process, while surface loading was maintained throughout the excavation process.

Table 2. HSS model parameters used for FE analysis.

γ_{sat} (kN/m³)	E_{50}^{ref} (kN/m²)	E_{oed}^{ref} (kN/m²)	E_{ur}^{ref} (kN/m²)	G_0^{ref} (kN/m²)
17.8	30,000	30,000	90,000	120,000
$\gamma_{0.7}$ -	C_{ref} (kN/m²)	ϕ' (°)	ν_{ur} -	R_f -
0.0002	0.05	35.4	0.3	0.9

3.2 Model validation

The finite element (FE) model was validated by comparing the predicted δ_w with field monitoring data reported by Hsiung et al. (2016). The referenced excavation was supported by a braced system with a H_{ex} of 16.8 m and four levels of steel struts. The computed depth profiles of δ_w in Figure 6 were found to be in good agreement with the measured data, with both results indicating a maximum wall deflection

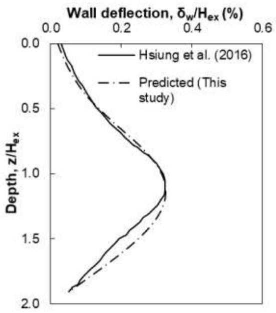

Figure 6. Validation of FE model (Hsiung et al. 2016).

($\delta_{w,m}$) of approximately 0.33%H_{ex} occurring near the final excavation level. The close agreement between measured and predicted wall deflections confirmed the reliability of the FE model for evaluating excavation-induced deformation under surface loading.

3.3 Effect of surface loading parameters

The maximum wall deflection ($\delta_{w,m}/H_{ex}$) from FE analysis for surface loading parameters were obtained and plotted in Figure 7. As shown in Figure 7(a), $\delta_{w,m}/H_{ex}$ was found to decrease with increasing e_s/H_{ex} and to approach the greenfield condition at e_s/H_{ex} = 1.2, indicating the limit influence range of loading distance from wall. The effect of e_s/H_{ex} was observed to be more pronounced for larger B_s/H_{ex}, and good agreement with centrifuge measurements. Figures 7(b) and (c) show that $\delta_{w,m}/H_{ex}$ increased with increasing B_s/H_{ex} and L_s/H_{ex}, respectively, with the influence of B_s/H_{ex} being larger due to the directional effect of loading width, while the effect of L_s/H_{ex} was restrained by wall corner stiffness. For B_s/H_{ex} and L_s/H_{ex} greater than 2.0, $\delta_{w,m}/H_{ex}$ were minimal, indicating limit size effects. As shown in Figure 7(d), $\delta_{w,m}/H_{ex}$ increased linearly with Q/Q_{ref} for smaller e_s/H_{ex}, whereas the influence of Q/Q_{ref} diminshed as the load was located

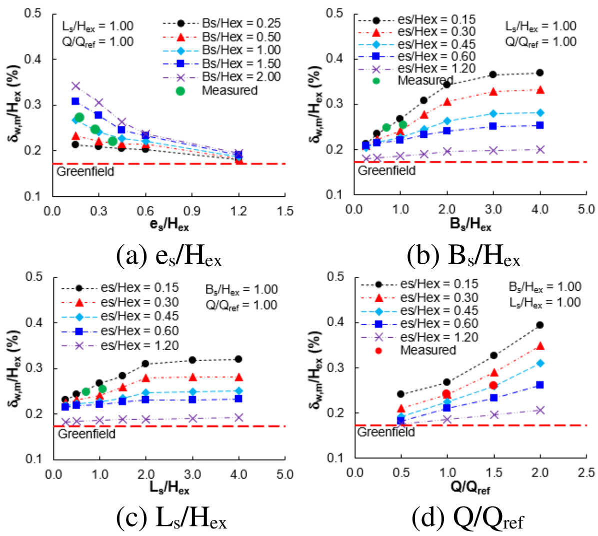

Figure 7. Values of $\delta_{w,m}/H_{ex}$ with loading parameters.

outside the wall influence zone. Although the surface settlement results are not presented, similar trends were observed, indicating a strong correlation between wall deflection and ground surface settlement behavior. The normalized trends are in good agreement, however, the distribution and absolute magnitude of wall displacement may differ due to differences in support installation mechanisms.

3.4 Design application for surface loading

The effects of surface loading components (e_s, B_s, L_s, and Q) were integrated into a unified design framework by modifying the system stiffness influence factor (I_F) by Abbas et al. (2024):

$$I_F = \frac{E_S}{p_A} \cdot \frac{E}{p_A} \cdot \frac{IA_S}{SP_h SP_v A_i} \cdot \frac{D}{H_{ex}} \qquad (1)$$

Where E_s and E = soil and wall elastic moduli; I = wall moment of inertia; A_s = strut area; H_{ex} and D = excavation and embedment depths; SP_h and SP_v = strut spacings; A_i = influence area; p_A = 100 kPa. Based on the observed influences of e_s, $A_{BL} = B_s \times L_s$, and Q on $\delta_{w,m}/H_{ex}$ and $s_{v,m}/H_{ex}$, a surface loading influence factor, η, was defined as:

$$\eta = I_F \times \frac{e_S^*}{A_{BL}^*} \times \frac{1}{Q^*} \qquad (2)$$

where $e_S^* = e_s/e_r$, $A_{BL}^* = A_{BL}/A_{BL,r}$ and $Q^* = Q/Q_{ref}$, with e_r = 1 m, $A_{BL,r}$ = 1 m^2, and Q_{ref} = 30 kPa. The formulation reflects the opposing effects of e_s versus A_{BL} and Q on excavation response. Unique correlations between η and $\delta_{w,m}/H_{ex}$ and $s_{v,m}/H_{ex}$ were obtained, as indicated in Figure 8(a) and (b), respectively. It should be noted that the proposed correlation was established for braced excavations using I_F with surface loading components, while the centrifuge results verified the fundamental loading behavior. The correlation was validated using published case histories and was found to be in good agreement, confirming the applicability of the proposed method.

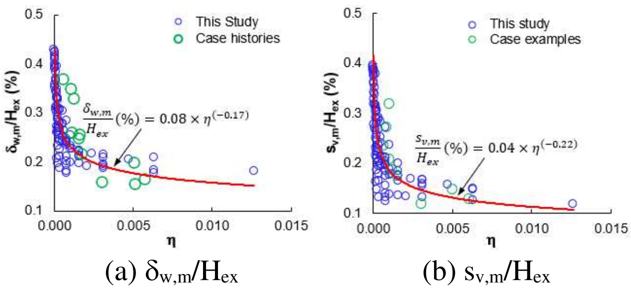

Figure 8. Correlative relationship of η with $\delta_{w,m}$ and $s_{v,m}$.

4 CONCLUSIONS

This study showed that surface loading significantly affects excavation-induced wall lateral deflection and ground surface settlement. Both $\delta_{w,m}/H_{ex}$ and $s_{v,m}/H_{ex}$ decreased with increasing e_s/H_{ex} and increased with increasing B_s/H_{ex} and L_s/H_{ex} and Q/Q_{ref}.The influence become negligible at e_s/H_{ex} = 1.2 and B_s/H_{ex}, L_s/H_{ex} = 2.0. B_s/H_{ex} showed a larger effect than L_s/H_{ex}, indicating directional sensitivity. A surface loading influence factor (η), derived from the stiffness influence factor (I_F), unified these effects and provided reliable predictions of wall deflection and surface settlement, as validated against published case histories.

ACKNOWLEDGEMENTS

The authors are grateful for the financial support provided by the Korea government (MSIT) through the NRF (Nos. RS-2025-00519983 and RS-2025-24683148) (KOPRI-PN25010)).

REFERENCES

Abbas, Q., Yoon, Y. and Lee, J. (2024). A method for characterizing stiffness of a support system for excavation design. *Int. Journal of Geomechanics, 24(2).* https://doi.org/10.1061/IJGNAI.GMENG-8687.

Abbas, Q., Yoon, Y., Shin, H. and Lee, J. (2025). Impact of surface loading on deep excavation response: Centrifuge and numerical analyses. *International Journal of Physical Modelling in Geotechnics, 25(1): 268-284*. https://doi.org/10.1680/jphmg.24.00083.

Brinkgreve, R., Engin, E., and Engin, H. (2010). Validation of empirical formulas to derive model parameters for sands. Numerical methods in geotechnical engineering, 137-142.

Goh, K. H., and Mair, R. J. (2014). Response of framed buildings to excavation-induced movements. *Soils and Foundations, 54(3): 250-268.* https://doi.org/10.1016/j.sandf.2014.04.002

Giraldo, J. R., and Bryson, L. S. (2021). Excavation support system design method to limit damage in adjacent infrastructure. *Journal Geotechnical and Geoenvironmental Engineering. Engineering, 147(12).* https://doi.org/10.1061/(ASCE)GT.1943-5606.0002677

Hsieh, P. O., and Ou, C. Y. (1998). Shape of ground surface settlement profiles caused by excavation. *Canadian Geotechnical Journal, 35(6).* https://doi.org/10.1139/t98-05.

Hsiung, B. C. B., Yang, K. H., Aila, W., Hung, C. (2016). Three-dimensional effects of a deep excavation on wall deflections in loose to medium dense sands. Computers and Geotechnics, 80: 138-151. https://doi.org/10.1016/j.compgeo.2016.07.001.

Li, L., Huang, J., and Han, B. (2018). Centrifugal investigation of excavation adjacent to existing composite foundation. Journal of Performance of Constructed Facilities, 32(3): 04018044. https://doi.org/10.1061/(ASCE)CF.1943-5509.0001188

Maddah, A., Soroush, A., and Shafipour, R., (2021). A new concept for interpretation of building-excavation interaction in 3D conditions. Tunnelling and Underground Space Technology, 109: 103757. https://doi.org/10.1016/j.tust.2020.103757.

Ou, X., Zhang, X., Fu, J., Zhang, C., Zhou, X., and Feng, H. (2020). Cause investigation of larger deformation of a deep excavation support system subjected to unsymmetrical surface loading. *Engineering Failure Analysis,107.* https://doi.org/10.1016/j.engfailanal.2019.104202

Son, M., and Cording, E.J., (2008). Evaluation of building stiffness for building response analysis to excavation-induced ground movements. *Journal Geotechnical and Geoenvironmental Engineering. 133, 995–1002.* https://doi.org/10.1061/(ASCE)1090-0241(2007)133:8(995)

Wang, X, Pan, Y., Chen, J., and Li, M. (2024). A spatiotemporal feature fusion-based deep learning framework for synchronous prediction of excavation stability. *Tunnelling and Underground Space Technology, 147: 105733.* https://doi.org/10.1016/j.tust.2024.105733.

Zhang, W., Hou, Z., Goh, A., and Zhang, R. (2019). Estimation of strut forces for braced excavation in granular soils from numerical analysis and case histories. Computers and Geotechnics, 106: 286-295. https://doi.org/10.1016/j.compgeo.2018.11.006.